ANTIMICROBIAL AGENTS AND CHEMOTHERAPY, May 2007, p. 1760–1769 Vol. 51, No. 5
0066-4804/07/$08.00+0 doi:10.1128/AAC.01267-06

Defining the Molecular Forces That Determine the Impact of Neomycin on Bacterial Protein Synthesis: Importance of the 2′-Amino Functionality▽†

Christopher M. Barbieri,[1] Malvika Kaul,[1] Melanie Bozza-Hingos,[1] Fang Zhao,[2] Yitzhak Tor,[2] Thomas Hermann,[2] and Daniel S. Pilch[1]*

Department of Pharmacology, University of Medicine and Dentistry of New Jersey-Robert Wood Johnson Medical School, 675 Hoes Lane, Piscataway, New Jersey 08854-5635,[1] and Department of Chemistry and Biochemistry, University of California, San Diego, 9500 Gilman Drive, La Jolla, California 92093-0358[2]

Received 10 October 2006/Returned for modification 4 January 2007/Accepted 4 March 2007

2-Deoxystreptamine (2-DOS) aminoglycosides exert their antibiotic actions by binding to the A site of the 16S rRNA and interfering with bacterial protein synthesis. However, the molecular forces that govern the antitranslational activities of aminoglycosides are poorly understood. Here, we describe studies aimed at elucidating these molecular forces. In this connection, we compare the bactericidal, antitranslational, and rRNA binding properties of the 4,5-disubstituted 2-DOS aminoglycoside neomycin (Neo) and a conformationally restricted analog of Neo (CR-Neo) in which the 2′-nitrogen atom is covalently conjugated to the 5″-carbon atom. The bactericidal potency of Neo exceeds that of CR-Neo, with this enhanced antibacterial activity reflecting a correspondingly enhanced antitranslational potency. Time-resolved fluorescence anisotropy studies suggest that the enhanced antitranslational potency of Neo relative to that of CR-Neo is due to a greater extent of drug-induced reduction in the mobilities of the nucleotides at positions 1492 and 1493 of the rRNA A site. Buffer- and salt-dependent binding studies, coupled with high-resolution structural information, point to electrostatic contacts between the 2′-amino functionality of Neo and the host rRNA as being an important modulator of 1492 and 1493 base mobilities and therefore antitranslational activities.

The increasing prevalence of multidrug-resistant bacterial infections has made the development of new antibiotics an important focus of current pharmacological research. A thorough understanding of the molecular mechanisms that underlie antibiotic action is an essential component of drug development. The 2-deoxystreptamine (2-DOS) aminoglycosides are potent bactericidal agents that target the 16S rRNA A site in the 30S ribosomal subunit, thereby interfering with bacterial protein synthesis (11, 12, 14, 31, 45).

Recent structural (11, 16–18, 33, 39, 41–43, 47) and biochemical (23, 46) studies have resulted in the proposal of a model for how aminoglycosides exert their deleterious effects on bacterial translation. This model is based on the premise that two conserved adenine residues at positions 1492 and 1493 of the rRNA A site play critical roles in the translation process. According to the model, A1492 and A1493 are in conformational equilibria between intrahelical and extrahelical states. When in their extrahelical states, A1492 and A1493 interact with the codon-anticodon minihelix. This interaction is favored in the presence of a cognate tRNA anticodon and disfavored in the presence of a noncognate tRNA anticodon. The binding of a 2-DOS aminoglycoside shifts the conformational equilibria of A1492 and A1493 toward the extrahelical state, thereby resulting in an enhanced interaction with the codon-anticodon minihelix, even when the tRNA anticodon is noncognate. The net results of this drug-induced effect are mistranslation, premature termination of translation, and inhibition of translation initiation (12). Consistent with this model for the antitranslational impact of aminoglycosides, we have previously shown that the extent of aminoglycoside-induced reduction in the mobilities of the bases at positions 1492 and 1493 of the A site is a more important determinant of bactericidal potency than the magnitude of drug affinity for the A site (25). However, the correlation between antitranslational activity and drug impact on 1492 and 1493 base mobilities has yet to be determined, with the same being true for the specific molecular forces that govern the mobilities of the 1492 and 1493 bases.

We describe here comparative studies of two aminoglycosides that exhibit markedly different bactericidal potencies. One of these compounds is the 4,5-disubstituted 2-DOS aminoglycoside neomycin (Neo), and the other is a conformationally restricted analog of Neo (CR-Neo) in which the 2′-nitrogen atom is covalently linked to the 5″-carbon atom, thereby conjugating rings II and III (Fig. 1). CR-Neo exhibits reduced bactericidal potency and affinity for the 16S rRNA A site relative to Neo (3, 8, 9, 48). However, differential affinity for the A site is not the likely basis for the differential antibacterial activities of the two drugs, since these two parameters are poorly correlated (1, 21, 25, 44). Our results indicate that the enhanced bactericidal potency of Neo relative to that of CR-Neo reflects a correspondingly enhanced antitranslational activity, which, in turn, correlates with an enhanced drug-induced

* Corresponding author. Mailing address: UMDNJ-Robert Wood Johnson Medical School, Department of Pharmacology, 675 Hoes Lane, Piscataway, NJ 08854-5635. Phone: (732) 235-3352. Fax: (732) 235-4073. E-mail: pilchds@umdnj.edu.

† Supplemental material for this article may be found at http://aac.asm.org/.

▽ Published ahead of print on 12 March 2007.

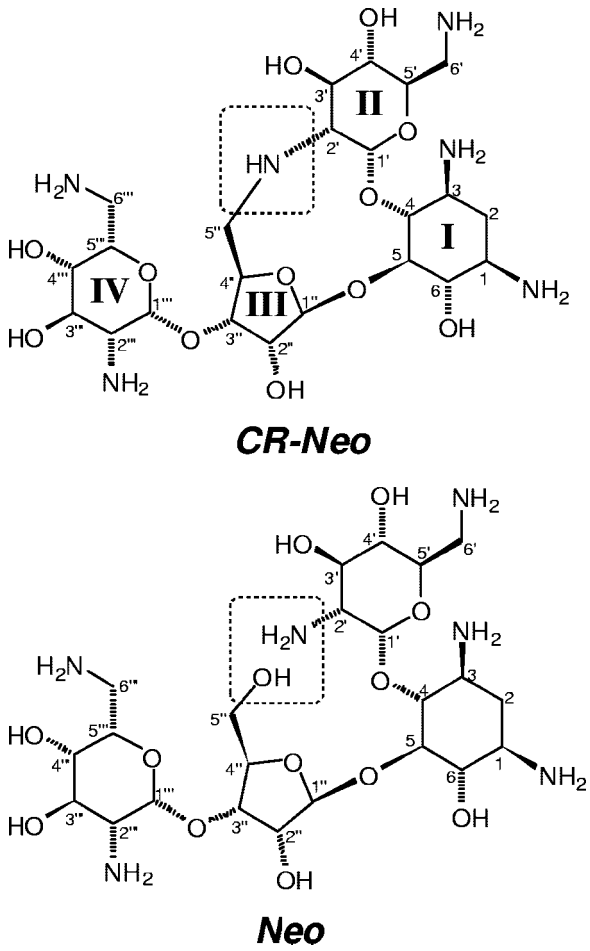

FIG. 1. Structures of Neo and CR-Neo in their deprotonated states, with the atomic and ring numbers indicated in Arabic and Roman numerals, respectively. The site of conformational restriction is boxed.

restriction of 1492 and 1493 base mobilities. In addition, our results highlight the importance of the 2′-amino functionality of Neo in determining the restrictive impact of the drug on 1492 and 1493 base mobilities.

MATERIALS AND METHODS

RNA and drug molecules. The RNA oligomers (Ec, Ec2AP1492, and Ec2AP1493) used in this study were obtained in their polyacrylamide gel electrophoresis-purified sodium salt forms from Dharmacon Research, Inc. (Lafayette, CO). The extinction coefficients at 260 nm and 85°C for the RNA oligomers were determined by enzymatic digestion and a subsequent colorimetric phosphate assay (36), which resulted in the following values {means ± standard deviations [in (mol of strand/liter)$^{-1}$ cm^{-1}]}: 253,390 ± 3,170 for Ec, 248,370 ± 940 for Ec2AP1492, and 235,140 ± 2,840 for Ec2AP1493. Neo · $3H_2SO_4$ · $3H_2O$ was obtained from Fluka (Milwaukee, WI). CR-Neo was synthesized in its trifluoroacetate form as previously described (9). The free base forms of both drugs were prepared as described in the following section.

Preparation of the free base forms of Neo and CR-Neo. Amberlite IRA-400 resin (Supelco, Bellefonte, PA) in its OH form (70 ml) was washed with 350 ml of distilled water. The washed resin was placed in a glass column 2.5 cm in diameter and 30 cm in length and washed with 50 ml of water. A 1-ml solution of 0.5 M Neo · $3H_2SO_4$ · $3H_2O$ was loaded onto the column. The free base form of the drug was then eluted from the column with 200 ml of water at a flow rate of 1 ml/min, and 30-ml fractions were collected. The pH of each fraction was measured, with the first three fractions having a pH of >9.0. These three fractions were pooled, lyophilized, and stored in their dry state at −20°C until used in the nuclear magnetic resonance (NMR) and calorimetric studies described below. CR-Neo free base was prepared in a manner identical to that of Neo free base, except that 4 ml of a 0.1 M solution of the CR-Neo trifluoroacetate salt was added to the washed IRA-400 resin.

ITC. Isothermal titration calorimetry (ITC) measurements were conducted at 25°C on a MicroCal VP-ITC (MicroCal, Inc., Northampton, MA). For the Neo experiments, 10-μl aliquots of 250 μM Neo were injected from a 250-μl rotating syringe (300 rpm) into an isothermal sample chamber containing 1.42 ml of an Ec solution that was 10 μM in strand. Each experiment of this type was accompanied by the corresponding control experiment, in which 10-μl aliquots of 250 μM Neo were injected into a solution of buffer alone. The duration of each injection was 10 seconds, and the initial delay prior to the first injection was 60 seconds. The delay between injections was 300 seconds. For the Neo experiments conducted at pH 7.5, the buffer solutions contained either 10 mM EPPS [*N*-(2-hydroxyethyl)piperazine-*N*′-(3-propanesulfonic acid)] or 10 mM TAPS [*N-tris*(hydroxymethyl)methyl-3-aminopropanesulfonic acid], 0.1 mM EDTA, and sufficient NaCl to bring the total Na^+ concentration to 100 mM. For the Neo experiments conducted at pH 9.0, the buffer solutions contained either 10 mM bicine or 10 mM TAPS, 0.1 mM EDTA, and sufficient NaCl to bring the total Na^+ concentration to 11 mM. For the CR-Neo experiments conducted at pH 7.5, 10-μl aliquots of 500 μM CR-Neo were injected from a 250-μl rotating syringe (300 rpm) into an Ec solution that was 20 μM in strand. The duration of each injection was 10 seconds, and the initial delay prior to the first injection was 60 seconds. The delay between injections was 600 seconds. In these experiments, the buffer solutions contained either 10 mM EPPS or 10 mM Tris, 0.1 mM EDTA, and sufficient NaCl to bring the total Na^+ concentration to 100 mM. For the CR-Neo experiments conducted at pH 9.0, seven 5-μl aliquots of 20 μM CR-Neo were injected into an Ec solution that was 20 μM in strand. In these experiments, the buffer solutions contained either 10 mM bicine or 10 mM TAPS, 0.1 mM EDTA, and sufficient NaCl to bring the total Na^+ concentration to 11 mM.

Each drug-RNA experiment was accompanied by the corresponding control experiment, in which the drug was injected into a solution of buffer alone. Each drug injection generated a heat burst curve (μcal/s versus s), the area under which was determined by integration (using Origin version 7.0 software [MicroCal, Inc., Northampton, MA]), to obtain a measure of the heat associated with that injection. The measure of the heat associated with each drug-buffer injection was subtracted from that of the corresponding heat associated with each drug-Ec injection to yield the heat of drug binding for that injection. The buffer-corrected ITC profiles for the binding of Neo to Ec at pH 7.5 and 9.0, as well as those for the binding of CR-Neo to Ec at pH 7.5, were fit with a model for two independent sets of binding sites. The binding parameters that emerged from these fits are listed in Table S1 in the supplemental material. We have previously assigned the first binding equilibrium to the specific A-site interaction observed in structural studies (18, 48) and the second binding equilibrium to weaker nonspecific interactions (24, 26, 27). The observed binding enthalpies (ΔH_{obs}) reported here reflect the enthalpies associated with the specific A-site binding reaction. The buffer-corrected measurements of the heat associated with injections 2 to 7 of CR-Neo into Ec at pH 9.0 were essentially identical. These heat measurements were averaged to yield relevant ΔH_{obs} values.

^{15}N NMR spectroscopy. ^{15}N NMR spectra were acquired at 30.4 MHz and 25°C on a Varian Unity 300 spectrometer using a recycle delay of 1 second. All ^{15}N chemical shifts are reported relative to those of NH_3 by using 1 M [^{15}N]urea in dimethyl sulfoxide (Isotec, Miamisburg, OH) as an external reference, with the ^{15}N chemical shift of the reference set to 77.0 ppm. The experimental NMR solutions were prepared by dissolving solid Neo or CR-Neo in 600 μl of 85% H_2O-15% D_2O to yield final drug concentrations between 100 and 500 mM. The pH of the NMR samples was adjusted by the addition of either HCl or KOH in 85% H_2O-15% D_2O. All pH measurements of NMR samples were acquired using a Corning 430 pH meter interfaced with a micro stem glass-calomel combination electrode (Mettler Toledo, Inc.). The assignments of the ^{15}N resonances were based on those previously reported (9, 10). Amine pK_a values were determined from plots of the pH dependence of ^{15}N chemical shifts by nonlinear least-squares analyses using the following relationship:

$$\delta = \frac{(\delta_{NH_2} - \delta_{NH_3^+})(10^{pH-pK_a})}{1 + (10^{pH-pK_a})} + \delta_{NH_3^+} \quad (1)$$

In this relationship, $\delta_{NH_3^+}$ and δ_{NH_2} are the ^{15}N chemical shifts of the amine nitrogens in their protonated and deprotonated states, respectively.

Steady-state fluorescence spectroscopy. Steady-state fluorescence experiments were conducted at 25°C on an Aviv model ATF105 spectrofluorometer (Aviv Biomedical, Lakewood, NJ) equipped with a thermoelectrically controlled cell

holder. The excitation wavelength was set at 310 nm in all the experiments, with the excitation and emission slit widths set at 5 nm. A quartz cell with a 1-cm path length in both the excitation and emission directions was used for all the measurements. In all titration experiments, 2- to 20-μl aliquots of solutions containing either Neo or CR-Neo (at concentrations ranging from 200 μM to 1.6 mM) were added sequentially to Ec2AP1492 solutions that were 1 μM in strand. After each addition, the sample was left to equilibrate for 3 minutes, whereupon the average emission intensity at 370 nm over a period of 30 seconds was recorded. The solution conditions for these experiments were 10 mM buffer (acetate at pH 5.0, EPPS at pH 7.5, and TAPS at pH 9.0), 0.1 mM EDTA, and sufficient NaCl to achieve the desired concentration of Na^+, which ranged from 11 to 430 mM. The average emission intensities at 370 nm of all samples were corrected by subtraction of the corresponding values for buffer alone. The fluorescence titration data were analyzed as previously described to yield drug-RNA association constants (K_a) (7, 25, 26).

Time-resolved fluorescence anisotropy. Time-resolved fluorescence anisotropy measurements were conducted at 25°C on a PTI EasyLife LS fluorescence lifetime system fitted with a 310-nm light-emitting diode light source, film polarizers in both the excitation and emission directions, and a 350-nm long-pass filter (Chroma Technology Corp., Rockingham, VT) in the emission direction. The slit width in the excitation direction was set at 6 mm. The fluorescence decay curves were acquired logarithmically in 400 channels with a 2-second integration time. The start and end delays of the acquisitions were 70 and 115 nanoseconds, respectively. The instrument response function was detected using light scattered by a dilute suspension of nondairy creamer, with the emission polarizer oriented parallel to the excitation polarizer and no cut-on filter in place. The RNA concentration was 20 μM in strand, and, when present, RNA-saturating concentrations of drug were employed (40 μM Neo and 100 μM CR-Neo). Each final decay profile reflected an average of four independent scans and was deconvolved in the Felix32 program (PTI, Inc.). These experiments were conducted in buffer containing 10 mM EPPS (pH 7.5), 0.1 mM EDTA, and sufficient NaCl to bring the total Na^+ concentration to 100 mM. The fluorescence intensity decays measured with the emission polarizer oriented either parallel [$I_{VV}(t)$] or perpendicular [$I_{VH}(t)$] to the excitation polarizer were best fit by the following sum of three exponentials:

$$I(t) = \sum_{i=1}^{3} \alpha_i e^{-t/\tau_i} \quad (2)$$

$I_{VV}(t)$ and $I_{VH}(t)$ were then deconvolved simultaneously with a magic angle decay [$D(t)$] using the following relationships:

$$I_{VV}(t) = \frac{D(t)[1 + 2r(t)]}{3}$$

$$I_{VH}(t) = \frac{D(t)[1 - r(t)]}{3G}$$

In these relationships, G is the instrumental correction factor and $r(t)$ is the anisotropy decay, which was best fit by the following sum of two exponentials:

$$r(t) = \beta_1 e^{-t/\phi_1} + \beta_2 e^{-t/\phi_2} \quad (3)$$

The limiting anisotropy at time zero [$r(0)$] was derived from the sum of β_1 and β_2. Values of G ranged from 0.90 to 1.11 and were determined using the following relationship:

$$G = \frac{\int I_{HV}(t)dt}{\int I_{HH}(t)dt}$$

In vitro transcription-translation assay. Differing concentrations of Neo and CR-Neo were combined with *E. coli* S30 extract containing nucleotide triphosphates (Promega, Madison, WI), a mixture of amino acids, and pBEST*luc* plasmid DNA (Promega) encoding the luciferase reporter protein. The reaction mixtures (50-μl final volume) were incubated at 37°C for 2 h and then cooled on ice for 10 min. Fifty microliters of dilution reagent (Promega) and 100 μl of SteadyGlow luciferin substrate (Promega) were then added, followed by incubation at room temperature for 5 min. The average light emission at 560 nm over a period of 30 seconds was recorded at 25°C using an Aviv ATF105 spectrofluorometer (Aviv Biomedical, Lakewood, NJ). A quartz cell with a 1-cm path length in the emission direction was used in these measurements, and the emission slit width was set at 10 nm. At least three replicate experiments were conducted at each drug concentration. Fifty percent inhibitory drug concentrations (IC_{50}) were determined by fitting semilogarithmic plots of translational efficiency (E), defined as the percentage of the translational level in the absence of drug, versus drug concentration ([D]) with the following sigmoidal dose-response relationship (where p is the Hill slope):

$$E = \frac{100}{\left(1 + \frac{[D]}{IC_{50}}\right)^p} \quad (4)$$

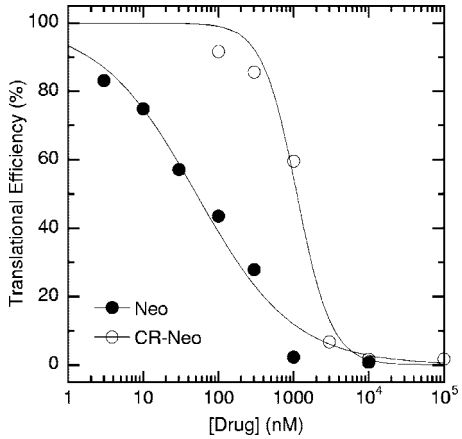

FIG. 2. Semilogarithmic plot of translational efficiency (defined as the percentage of the translational level in the absence of drug) as a function of Neo and CR-Neo concentrations. Each data point represents an average for at least three independent experiments. The solid lines represent fits of the experimental data with equation 4.

Antibacterial assay. Antibacterial activities were determined using a standard broth dilution assay (2). *E. coli* DH5α cells in log phase were grown at 37°C in Luria-Bertani (LB) medium containing twofold serial dilutions of Neo or CR-Neo to yield final concentrations ranging from 2.0 mM to 10 nM. Bacterial growth was monitored after 24 h by measuring the optical density at 620 nm, with the MIC being defined as the lowest drug concentration at which growth is completely inhibited. Antibacterial activities were assayed in at least three independent experiments, with each experiment including three replicates of each drug concentration.

RESULTS AND DISCUSSION

The antibacterial activities of Neo and CR-Neo correlate with their antitranslational activities in vitro. We compared the bactericidal activities of Neo and CR-Neo versus *E. coli* DH5α cells. Neo (MIC = 1.9 mg/liter) kills these bacterial cells with an ~60-fold-greater potency than CR-Neo (MIC = 119 mg/liter). Similar differential patterns of bactericidal activity have also been observed versus the BL21 and ATCC 25992 standard strains of *E. coli* (3, 8, 48). Recall that the accepted mechanism by which aminoglycosides exert their antibiotic actions is through their deleterious effects on protein synthesis. We therefore sought to determine whether the enhanced bactericidal activity of Neo relative to that of CR-Neo reflects a correspondingly enhanced antitranslational activity. To this end, we monitored the impact of Neo and CR-Neo on the expression of the luciferase protein by using an *E. coli* S30 extract transcription-translation system. Figure 2 shows the resulting protein synthesis inhibition data. Inspection of these data reveals that Neo (IC_{50} = 50 ± 9 nM) is 22-fold more potent at inhibiting translation than CR-Neo (IC_{50} = 1,100 ± 132 nM). This result is consistent with the enhanced antibacterial activity of Neo relative to that of CR-Neo being due to an enhanced ability to inhibit protein synthesis.

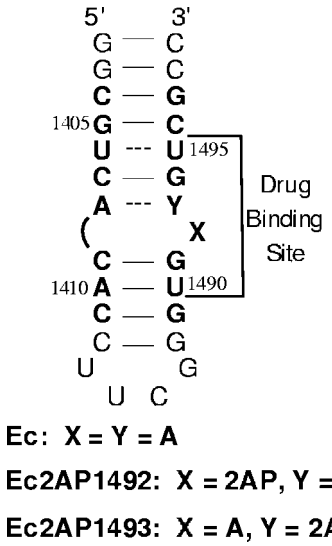

FIG. 3. Secondary structure of the *E. coli* 16S rRNA A-site model oligonucleotide (Ec). Ec differs from Ec2AP1492 and Ec2AP1493 with respect to the identity of the base at position 1492 or 1493 (denoted by X or Y, respectively). The bases at both positions 1492 and 1493 are adenines in Ec, with the 1492 base being 2AP in Ec2AP1492 and the 1493 base being 2AP in Ec2AP1493. Watson-Crick base pairs are denoted by solid lines, while mismatched base pairs are denoted by dashed lines. Bases present in *E. coli* 16S rRNA are depicted in boldface and are numbered as they are in the 16S rRNA. The drug binding site is indicated.

The binding of Neo to the 16S rRNA A site reduces the mobilities of the bases at positions 1492 and 1493 to a greater extent than the binding of CR-Neo. We have previously suggested that aminoglycoside-induced reduction in the mobilities of the bases at positions 1492 and 1493 of the 16S rRNA A site is a potentially key determinant of bactericidal activity as mediated through antitranslational effects (25). Thus, one would expect the differential antitranslational activities of CR-Neo and Neo to be correlated with correspondingly different extents of binding-induced reduction in the mobilities of the 1492 and 1493 bases. We probed for this correlation by using time-resolved fluorescence anisotropy techniques to compare and contrast the impacts of Neo and CR-Neo binding on the conformational dynamics of an RNA oligonucleotide construct (Ec) that has been shown to be an effective model of the *E. coli* 16S rRNA A site (Fig. 3) (30, 37). For these fluorescence experiments, the adenine residue at position 1492 or 1493 of Ec was substituted with the fluorescent base analog 2-aminopurine (2AP), with the resulting 2AP-substituted oligomers being designated Ec2AP1492 and Ec2AP1493, respectively. Figure 4 shows a representative set of polarized fluorescence intensity decays for Ec2AP1492 (A) and Ec2AP1493 (D) and their complexes with Neo (B and E) and CR-Neo (C and F), with the emission polarizer oriented either parallel (I_{VV}) or perpendicular (I_{VH}) to the excitation polarizer. All the polarized fluorescence intensity decays were deconvolved as described in Materials and Methods to yield the anisotropy decay parameters listed in Table 1. The anisotropy decays are best described as the sum of two exponential terms (equation 3). The $r(0)$ values for the biexponential fits range from 0.266 to 0.356, in good agreement with previously reported $r(0)$ values for 2AP in both DNA and RNA, which ranged from 0.266 to 0.377 (22, 25, 32, 40).

The longer of the two rotational correlation times (ϕ_1) reflects the overall tumbling of the RNA duplex, while the shorter rotational correlation time (ϕ_2) reflects the internal motion of the 2AP base in the RNA (25). Thus, a drug-induced increase in ϕ_2 reflects a corresponding decrease in 2AP base mobility. Note that the binding of Neo to both Ec2AP1492 and Ec2AP1493 increases ϕ_2 to a greater extent (1.87 and 1.55 nanoseconds for Ec2AP1492 and Ec2AP1493, respectively) than the binding of CR-Neo (0.28 and 0.24 nanoseconds for Ec2AP1492 and Ec2AP1493, respectively). These results indicate that the binding of Neo decreases the mobilities of the bases at positions 1492 and 1493 to a greater extent than the binding of CR-Neo. Thus, the differential antitranslational activities of CR-Neo and Neo do indeed correlate with the differing extents to which their binding reduces the mobilities of the 1492 and 1493 bases.

The binding of Ec to Neo is linked to a greater extent of drug protonation than the binding of Ec to CR-Neo. While the time-resolved fluorescence anisotropy studies described in the previous section reveal the impact of Neo and CR-Neo binding on the mobilities of the 1492 and 1493 bases, they do not provide information about the molecular forces that dictate these drug-induced changes in base mobility. As a first step toward elucidating the relevant molecular forces, we probed for Ec binding-induced increases in the basicities (pK_a values) of the Neo and CR-Neo drug amine groups (i.e., shifts in the equilibria of the amine groups from their uncharged states to their fully protonated cationic states). Such alterations in amine group basicity result in the coupling of drug protonation to the RNA binding reaction. We used ITC to characterize the binding of Neo and CR-Neo to Ec in two different buffers that differ with respect to their heat of ionization (ΔH_{ion}). When binding and protonation are linked, which can occur only under pH conditions where the amine groups of the unbound drug molecules are not in their fully protonated states (pH > 5.0), the observed binding enthalpies (ΔH_{obs}) will differ between the two buffers. Moreover, the number of protons linked to binding at a specific pH (Δn) can be determined by simultaneous solution of the following two equations (15):

$$\Delta H_{obs1} = \Delta H_{corr} + \Delta n(\Delta H_{ion1}) \quad (5)$$

$$\Delta H_{obs2} = \Delta H_{corr} + \Delta n(\Delta H_{ion2}) \quad (6)$$

In these equations, the numerical subscripts refer to the different buffers and ΔH_{corr} reflects the observed binding enthalpy corrected for buffer ionization effects. Figure 5 shows the ITC profiles for the binding of Neo (A to C) and CR-Neo (D to F) to Ec at pH 7.5. The Neo titrations were conducted in the presence of either TAPS (ΔH_{ion} = +9.92 kcal/mol) or EPPS (ΔH_{ion} = +5.15 kcal/mol) buffer, while the CR-Neo titrations were conducted in the presence of either Tris (ΔH_{ion} = +11.34 kcal/mol) or EPPS buffer. We used Tris rather than TAPS buffer in our CR-Neo titrations at pH 7.5, since the binding of CR-Neo at this pH was essentially undetectable calorimetrically in TAPS buffer (i.e., ΔH_{obs} was essentially zero under these particular buffer conditions). Each of the heat burst curves in Fig. 5A, B, D, and E corresponds to a single drug injection. The heats derived from the integration of

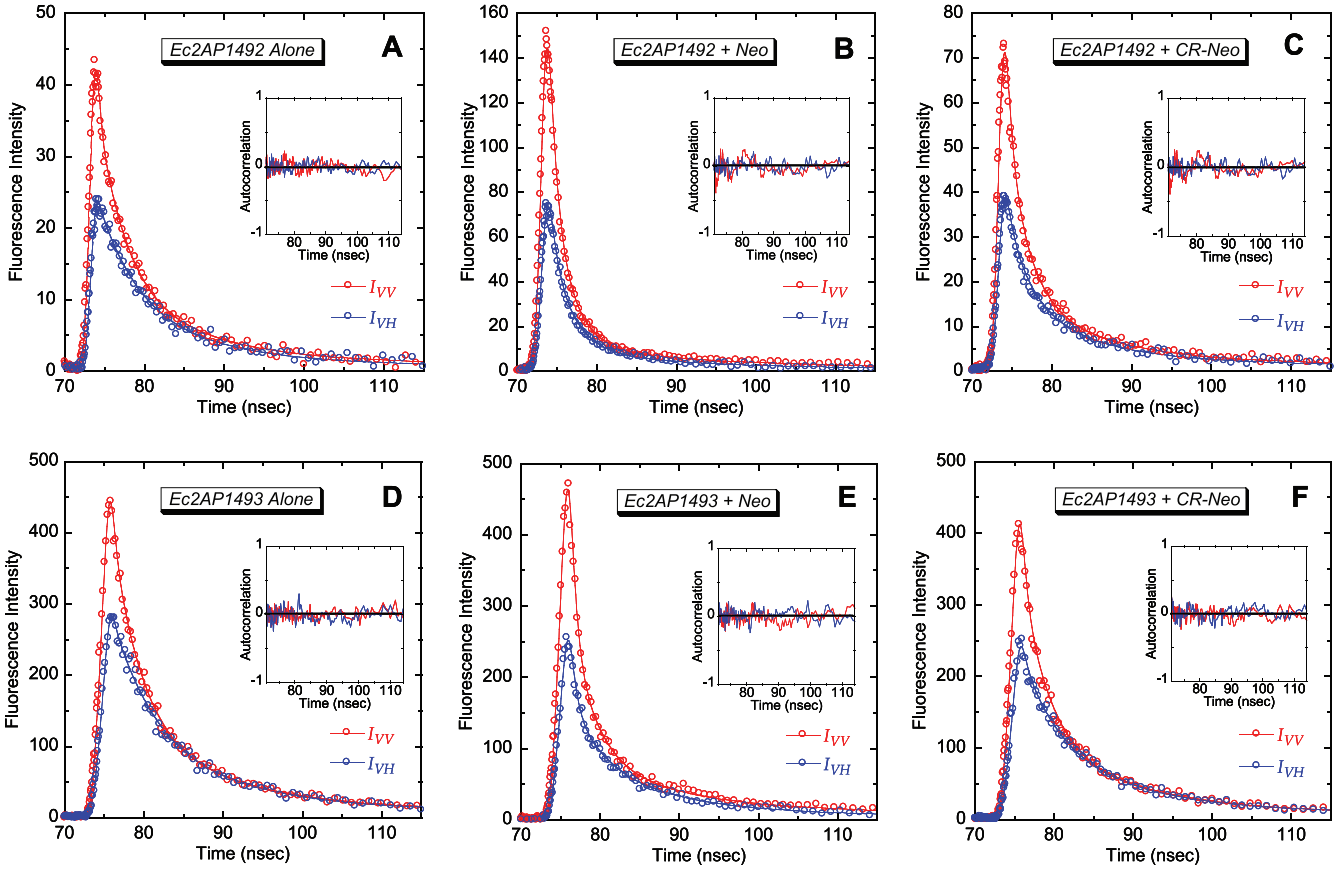

FIG. 4. Polarized fluorescence intensity decay profiles at 25°C for Ec2AP1492 (A) and Ec2AP1493 (D) and their complexes with Neo (B and E) and CR-Neo (C and F). The decay profile with the emission polarizer oriented parallel to the excitation polarizer (I_{VV}) is depicted in red, while the decay profile with the emission polarizer oriented perpendicular to the excitation polarizer (I_{VH}) is depicted in blue. In each panel, the hollow circles represent the experimental data points, while the solid lines reflect the nonlinear least-squares fits of the data with equation 2. The inset in each panel shows the autocorrelation functions of the weighted residuals for the fits of the corresponding decay profiles. The solution conditions were 10 mM EPPS (pH 7.5), 0.1 mM EDTA, and sufficient NaCl to bring the total Na^+ concentration to 100 mM. nsec, nanoseconds.

these heat burst curves were corrected for drug dilution effects as described in Materials and Methods, with the resulting corrected injection heats shown in Fig. 5C and F.

In both drug titrations, the magnitude of the exothermic signal is substantially greater in EPPS buffer than in the other buffers employed (TAPS for Neo and Tris for CR-Neo). This observation indicates that the binding of both Neo and CR-Neo to Ec is coupled to drug protonation (5, 6, 24, 27, 34, 35). Table 2 lists the ΔH_{obs} values derived from fits of the corrected injection heat profiles shown in Fig. 5C and F as described in Materials and Methods. In addition, Table 2 also lists the corresponding values of Δn and ΔH_{corr} calculated using equations 5 and 6. Inspection of these data reveals Δn values of 1.61 ± 0.05 for Neo and 1.29 ± 0.03 for CR-Neo. Note that these Δn values reflect contributions from all drug amine groups whose protonation is linked to Ec binding, which, at pH 7.5, number at least two for each drug, since Δn is >1.0. Furthermore, Neo exhibits a greater degree of binding-linked protonation than CR-Neo. This enhanced protonation contributes to the more exothermic ΔH_{corr} value associated with the

TABLE 1. Fluorescence anisotropy decay parameters for Ec2AP1492 and Ec2AP1493 and their complexes with Neo and CR-Neo at 25°C[a]

RNA	Drug	β_1	ϕ_1 (ns)	β_2	ϕ_2 (ns)	$r(0)$[b]
Ec2AP1492	None	0.192 ± 0.014	3.68 ± 1.17	0.139 ± 0.069	0.48 ± 0.03	0.331 ± 0.083
Ec2AP1492	Neo	0.053 ± 0.006	7.32 ± 1.95	0.213 ± 0.003	2.35 ± 0.28	0.266 ± 0.009
Ec2AP1492	CR-Neo	0.203 ± 0.047	4.38 ± 1.78	0.105 ± 0.017	0.76 ± 0.11	0.308 ± 0.064
Ec2AP1493	None	0.200 ± 0.010	5.97 ± 1.53	0.156 ± 0.059	0.41 ± 0.01	0.356 ± 0.069
Ec2AP1493	Neo	0.208 ± 0.015	5.32 ± 0.72	0.065 ± 0.023	1.96 ± 0.07	0.273 ± 0.071
Ec2AP1493	CR-Neo	0.208 ± 0.005	3.95 ± 0.97	0.081 ± 0.026	0.65 ± 0.04	0.288 ± 0.031

[a] For each sample, the values of β_1, ϕ_1, β_2, and ϕ_2 represent means ± standard deviations for at least two independent experiments.
[b] Values of $r(0)$ were calculated from the sum of β_1 and β_2, with the indicated uncertainties reflecting the maximum possible errors as propagated through this summation.

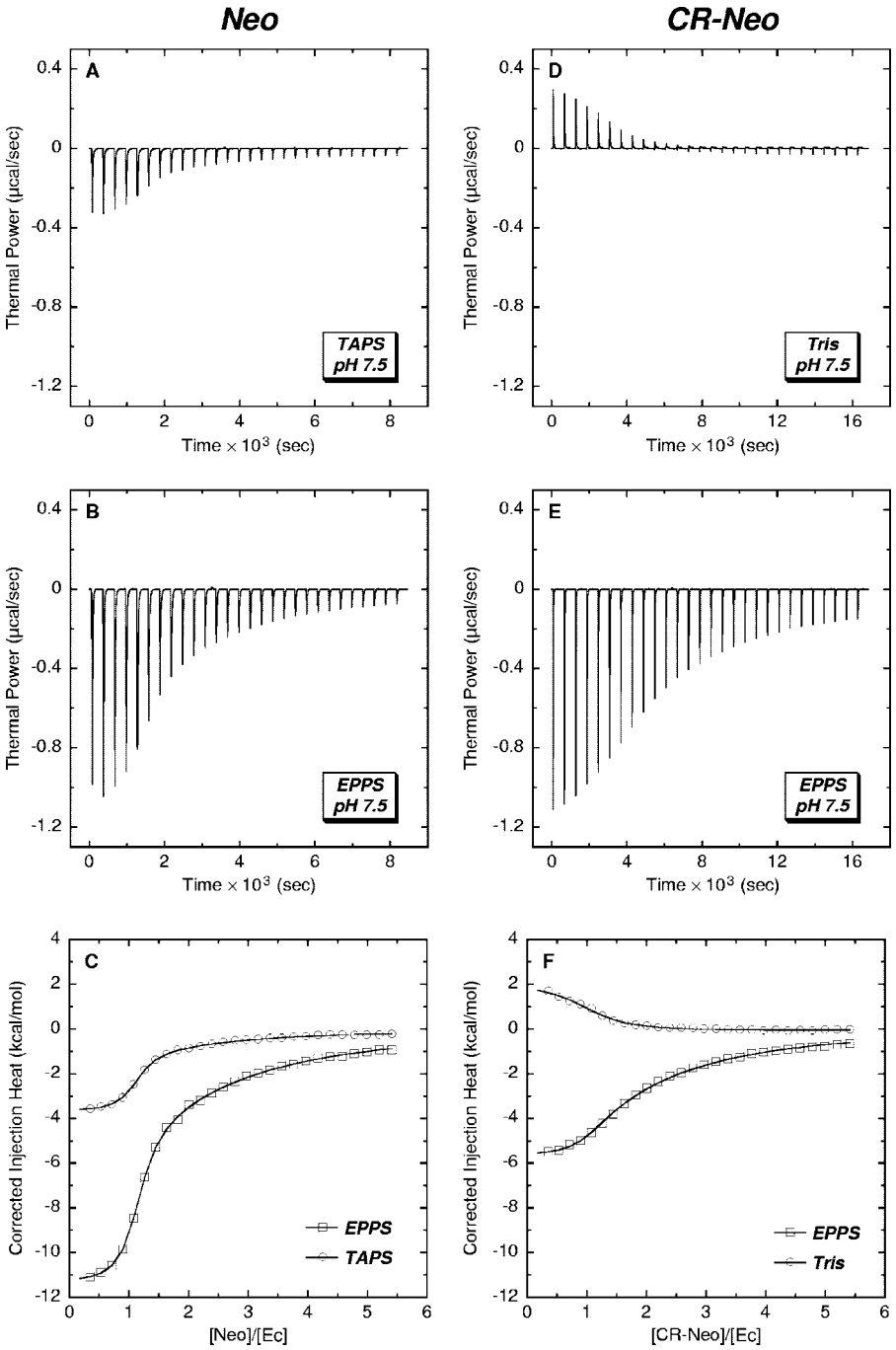

FIG. 5. ITC profiles at 25°C for the titration of either Neo (A to C) or CR-Neo (D to F) into a solution of Ec at pH 7.5 in the presence of TAPS (A), EPPS (B and E), or Tris (D) buffer. Each heat burst curve in panels A and B is the result of a 10-μl injection of 250 μM Neo into a solution of Ec that was 10 μM in strand. Each heat burst curve in panels D and E is the result of a 10-μl injection of 500 μM CR-Neo into a solution of Ec that was 20 μM in strand. The solution conditions were as described in the legend to Fig. 4. The data points in panels C and F reflect the buffer-corrected experimental injection heat values, while the solid lines reflect the calculated fits of the data by using a model for two sets of binding sites.

binding of Neo than that associated with the binding of CR-Neo.

In addition to RNA binding-linked protonation data acquired at pH 7.5, Table 2 also lists the corresponding data acquired at pH 9.0. The two buffers used in the experiments conducted at pH 9.0 were bicine ($\Delta H_{ion} = +6.47$ kcal/mol) and TAPS. Note that for both drugs, the magnitudes of Δn and ΔH_{corr} are greater at pH 9.0 than at pH 7.5, an observation consistent with an increased amount of binding-linked drug protonation at the higher pH. The Δn values for Neo and CR-Neo at pH 9.0 (2.84 ± 0.06 and 2.32 ± 0.06, respectively) are consistent with the binding of each drug to Ec being linked

TABLE 2. Number of protons coupled to the binding of Neo and CR-Neo to Ec

Drug	pH	Buffer	ΔH_{ion} (kcal/mol)[a]	ΔH_{obs} (kcal/mol)	ΔH_{corr} (kcal/mol)[b]	Δn[b]
Neo	7.5	EPPS	+5.15	−11.4 ± 0.1	−19.7 ± 0.3	1.61 ± 0.05
		TAPS	+9.92	−3.7 ± 0.1		
CR-Neo	7.5	EPPS	+5.15	−6.0 ± 0.1	−12.7 ± 0.3	1.29 ± 0.03
		Tris	+11.34	+2.0 ± 0.1		
Neo	9.0	Bicine	+6.47	−14.9 ± 0.1	−33.3 ± 0.5	2.84 ± 0.06
		TAPS	+9.92	−5.1 ± 0.1		
CR-Neo	9.0	Bicine	+6.47	−9.6 ± 0.1	−24.6 ± 0.5	2.32 ± 0.06
		TAPS	+9.92	−1.6 ± 0.1		

[a] ΔH_{ion} values at 25°C for the indicated buffers were taken from Fukada and Takahashi (20).
[b] ΔH_{corr} and Δn values were calculated from the values of ΔH_{obs} by using equations 5 and 6, with the indicated uncertainties reflecting the maximum possible errors in ΔH_{obs} as propagated through these equations.

to protonation of three amine groups. These Δn values also indicate that the pK_a values of the relevant drug amine groups in the RNA-bound drugs must be >9.0. Asensio and coworkers observed similar pK_a increases accompanying the binding of Neo to its specific RNA aptamer (19).

The number of Neo and CR-Neo amine groups that participate in electrostatic interactions with Ec varies with pH. The Ec binding-linked protonation studies described in the preceding section highlight the importance of electrostatic interactions in driving the formation of the drug-Ec complexes, since such interactions can provide the necessary energy to overcome the energetic cost that is known to be associated with binding-linked ligand protonation reactions (i.e., binding-induced increases in ligand pK_a) (4, 13, 15, 24, 27, 28, 34, 35). We quantitatively assessed these electrostatic contributions to the Ec binding of Neo and CR-Neo by monitoring the salt dependence of the drug-RNA binding constants (K_a). The salt dependence of K_a can be analyzed according to the polyelectrolyte theories of Manning (29) and Record et al. (38), which invoke the linkage between the nucleic acid binding of a positively charged drug molecule and the release of counterions (e.g., Na^+ ions) from a condensed state surrounding the nucleic acid to a free state in solution. This binding-induced release of counterions provides an entropically favorable contribution to the binding free energy.

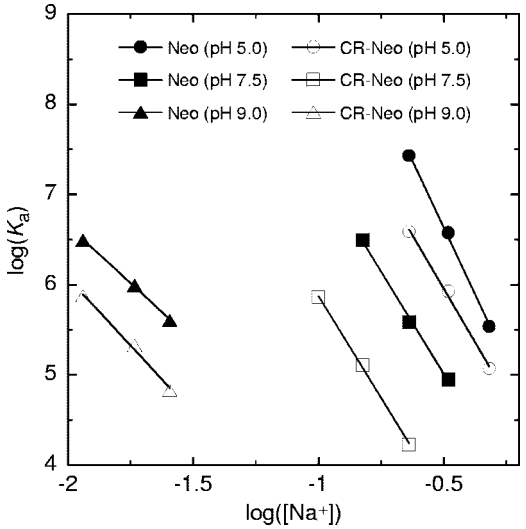

FIG. 6. $Log(K_a)$ versus $log([Na^+])$ plots for the binding of Neo and CR-Neo to Ec2AP1492 at pH 5.0, 7.5, and 9.0. The experimental data points were fit by linear regression, with the resulting fits depicted as solid lines.

Figure 6 shows plots of $log(K_a)$ versus $log([Na^+])$ for the binding of both Neo and CR-Neo to Ec2AP1492 at pH values of 5.0, 7.5, and 9.0. This range of pH values ensures that the salt dependencies of the drug-RNA binding reactions whose results are shown in Fig. 6 reflect conditions under which the protonation states of the unbound drugs range from essentially fully protonated to significantly deprotonated. Note the linearity of the $log(K_a)$-versus-$log([Na^+])$ plots. The slope of each plot yields the following quantity (38):

$$\frac{\partial \log(K_a)}{\partial \log([M^+])} = -Z\psi$$

In this relationship, $[M^+]$ is monovalent cation concentration, Z denotes the apparent charge on the RNA-bound drug, and ψ is the fraction of M^+ bound per nucleic acid phosphate. The value of ψ for the A-form poly(rA) · poly(rU) duplex is 0.89, while that for single-stranded poly(rA) is 0.78 (38). The ψ value for the internal loop region of the 16S rRNA A site may lie between these two values.

Linear regression analyses of the plots in Fig. 6 yield the $Z\psi$ values listed in Table 3. At pH 5.0, the $Z\psi$ values associated with the binding of Neo and CR-Neo to Ec2AP1492 are 5.9 ± 0.3 and 4.7 ± 0.3, respectively. Thus, under conditions where

TABLE 3. Electrostatic contributions to the binding of Neo and CR-Neo to Ec2AP1492 at pH 5.0, 7.5, and 9.0[a]

Drug	$Z\psi$ at pH:		
	5.0	7.5	9.0
Neo	5.9 ± 0.3	4.5 ± 0.3	2.6 ± 0.1
CR-Neo	4.7 ± 0.3	4.5 ± 0.1	3.0 ± 0.2

[a] Values of $Z\psi$ were calculated from the slopes of the linear fits of the $log(K_a)$-versus-$log([Na^+])$ plots shown in Fig. 6, with the indicated uncertainties reflecting the standard deviations of the fitted lines from the experimental points.

both drugs are essentially fully protonated, all six charged amine groups of Neo participate in electrostatic interactions with the host RNA, but only five of the six charged amine groups of CR-Neo are engaged in such interactions. The latter observation indicates that the presence of a positively charged amine functionality on an aminoglycoside does not necessarily imply that it will form favorable electrostatic contacts with a target RNA.

Upon an increase in pH from 5.0 to 7.5, the $Z\psi$ value of Neo decreases from 5.9 ± 0.3 to 4.5 ± 0.3. By contrast, the $Z\psi$ value of CR-Neo remains essentially unchanged (4.7 ± 0.3 versus 4.5 ± 0.1). Thus, Neo binding loses favorable electrostatic contributions from one amine group with a pH increase from 5.0 to 7.5, while the electrostatic contributions to CR-Neo binding remain unchanged over this pH range. The Neo results indicate that the deprotonation of one amine group that accompanies a pH increase from 5.0 to 7.5 abolishes the electrostatic contributions of that functionality to RNA binding, which, in turn, implies that the protonation of this functionality is not linked to the binding reaction. In other words, the pK_a of this amine functionality is not increased upon RNA binding, even though the protonated cationic form of the amine group is capable of engaging in electrostatic interactions with the host RNA.

A pH increase from 7.5 to 9.0 causes the $Z\psi$ value of Neo to decrease from 4.5 ± 0.3 to 2.6 ± 0.1, while causing the $Z\psi$ value of CR-Neo to decrease from 4.5 ± 0.1 to 3.0 ± 0.2. These results indicate that the number of Neo and CR-Neo amine groups that afford favorable electrostatic contributions to RNA binding decreases from five to three with a pH increase from 7.5 to 9.0. Note the agreement between the number (three) of Neo and CR-Neo amine groups engaged in electrostatic interactions with the host RNA at pH 9.0 and the corresponding number of drug amines whose protonation we found to be linked to Ec binding at this pH. This gratifying concordance establishes the involvement of three Neo and CR-Neo amine groups in electrostatic contacts that are critical for the stabilization of the drug-RNA complex. In order to determine the identities of these drug amine groups, one must know the pK_a values of all the drug amine functionalities. In the section that follows, we describe how we determined the requisite pK_a values.

Determination of the pK_a values for the amine groups of the free base forms of Neo and CR-Neo by using natural abundance ^{15}N NMR. We monitored the pH dependencies of the ^{15}N NMR chemical shifts of the free base forms of Neo and CR-Neo, with the resulting pH profiles shown in Fig. S1 in the supplemental material. Estimates for the pK_a values of the drug amines were determined from nonlinear least-squares fits of the pH profiles using equation 1. The resulting pK_a values are listed in Table 4, with the corresponding values of $\delta_{NH_3^+}$ and δ_{NH_2} that emerged from these fits listed in Table S2 in the supplemental material. The pK_a values of Neo range from 6.2 to 9.1, while the pK_a values of CR-Neo range from 6.2 to 9.2. Not surprisingly, the amine most affected by the conformational restriction is the 2′-amine, since this group is directly involved in cyclization with the 5″-group (Fig. 1). In this regard, the pK_a of the 2′-amine group of CR-Neo (6.4) is 1.4 units lower than that of Neo (7.8). It has previously been suggested that this reduced basicity reflects a constricted structural context that hinders the solvation of the protonated cationic state (9). In contrast to its impact on the pK_a of the 2′-amine, the conformational restriction increases the pK_a values of the 1-, 6′-, 2‴-, and 6‴-amino groups by 0.1 to 0.4 units.

TABLE 4. ^{15}N NMR-derived pK_a values for the amine groups of the free base forms of Neo and CR-Neo at 25°C[a]

Amine group	pK_a (±0.1) for:	
	Neo	CR-Neo
1	8.1	8.5
3	6.2	6.2
2′	7.8	6.4
6′	8.8	9.0
2‴	7.8	8.0
6‴	9.1	9.2

[a] pK_a values were derived from fits of the pH-dependent ^{15}N chemical shift data shown in Fig. S1 in the supplemental material using equation 1.

Protonation of the 2′-amine group is linked to the binding of Ec to Neo but not to CR-Neo. A comparison of the Δn values listed in Table 2 with the corresponding protonation states of Neo and CR-Neo predicted by the NMR-derived pK_a values listed in Table 4 enables us to identify the specific drug amine groups whose protonation is linked to Ec binding. These determinations indicate that the binding of Neo to Ec is coupled to protonation of the 3-, 2′-, and 2‴-amine functionalities, while the binding of CR-Neo is coupled to protonation of the 3-, 2‴-, and 6‴-amine groups. Note that protonation of the 2′-amine group is linked to the binding of Ec to Neo but not to CR-Neo. This observation suggests that the RNA contacts formed by the 2′-amine group differ between the Neo-rRNA complex and the CR-Neo–rRNA complex. In support of this possibility, a comparison of recently reported (18, 48) crystal structures of Neo (Protein Data Bank codes 2AO4 and 2ET4) and CR-Neo (Protein Data Bank code 1ZZ5) in complex with 16S rRNA A-site model RNA oligomers reveals a key contact that is present in the Neo-rRNA complex but absent in the CR-Neo–rRNA complex. Significantly, this contact is an electrostatic interaction between the 2′-amine group of Neo and the phosphate functionality of A1492. Recall our salt-dependent binding data acquired at pH 5.0, which revealed that only five of the six charged CR-Neo amine groups form electrostatic contacts with Ec2AP1492. The structural database suggests that the sole CR-Neo functionality not electrostatically engaged at this pH is the 2′-amine group. The absence of an electrostatic contact between the CR-Neo 2′-amine group and the phosphate functionality of A1492 may also account for the reduced affinity exhibited by CR-Neo relative to that exhibited by Neo for the 16S rRNA A site (Fig. 6) (9).

Potential role for the 2′-amino group in determining the impact of Neo on 1492 and 1493 base mobility and thus antitranslational activity. It is likely that the interaction between the drug 2′-amino group and the phosphate functionality of A1492 not only enhances the stability of the drug-rRNA complex but also restricts the mobility of the 1492 base. In fact, this interaction may also serve to restrict the mobility of the 1493 base, given its proximal location to the 1492 base along the RNA backbone. Such restrictions would account for the fact that Neo binding reduces the mobilities of the 1492 and 1493

bases to greater extents than does the binding of CR-Neo (Table 1). In the aggregate, our results suggest that the 2′-amino group of Neo plays a key role in determining the antitranslational properties of the drug by virtue of its role in restricting the mobilities of the 1492 and 1493 bases of the 16S rRNA A site. This information should prove useful in directing future efforts aimed at the design of next-generation antibiotics that target the bacterial rRNA A site.

ACKNOWLEDGMENTS

This work was supported by NIH grants CA097123 (D.S.P.), AI47673 (Y.T.), and AI51104 (T.H.). C.M.B. was supported in part by an NIH training grant (5T32 GM08319) in molecular biophysics. M.K. was supported in part by an NIH postdoctoral fellowship (F32 AI62041).

REFERENCES

1. **Alper, P. B., M. Hendrix, P. Sears, and C.-H. Wong.** 1998. Probing the specificity of aminoglycoside-ribosomal RNA interactions with designed synthetic analogs. J. Am. Chem. Soc. **120:**1965–1978.
2. **Andrews, J. M.** 2001. Determination of minimum inhibitory concentrations. J. Antimicrob. Chemother. **48**(Suppl. 1)**:**5–16.
3. **Asensio, J. L., A. Hidalgo, A. Bastida, M. Torrado, F. Corzana, J. L. Chiara, E. García-Junceda, J. Cañada, and J. Jiménez-Barbero.** 2005. A simple structural-based approach to prevent aminoglycoside inactivation by bacterial defense proteins: conformational restriction provides effective protection against neomycin B nucleotidylation by ANT4. J. Am. Chem. Soc. **127:**8278–8279.
4. **Baker, B. M., and K. P. Murphy.** 1996. Evaluation of linked protonation effects in protein binding reactions using isothermal titration calorimetry. Biophys. J. **71:**2049–2055.
5. **Barbieri, C. M., T.-K. Li, S. Guo, G. Wang, A. J. Shallop, W. Pan, G. Yang, B. L. Gaffney, R. A. Jones, and D. S. Pilch.** 2003. Aminoglycoside complexation with a DNA·RNA hybrid duplex: the thermodynamics of recognition and inhibition of RNA processing enzymes. J. Am. Chem. Soc. **125:**6469–6477.
6. **Barbieri, C. M., and D. S. Pilch.** 2006. Complete thermodynamic characterization of the multiple protonation equilibria of the aminoglycoside antibiotic paromomycin: a calorimetric and natural abundance ^{15}N NMR study. Biophys. J. **90:**1338–1349.
7. **Barbieri, C. M., A. R. Srinivasan, and D. S. Pilch.** 2004. Deciphering the origins of observed heat capacity changes for aminoglycoside binding to prokaryotic and eukaryotic ribosomal RNA A-sites: a calorimetric, computational, and osmotic stress study. J. Am. Chem. Soc. **126:**14380–14388.
8. **Bastida, A., A. Hidalgo, J. L. Chiara, M. Torrado, F. Corzana, J. M. Pérez-Cañadillas, P. Groves, E. García-Junceda, C. Gonzalez, J. Jiménez-Barbero, and J. L. Asensio.** 2006. Exploring the use of conformationally locked aminoglycosides as a new strategy to overcome bacterial resistance. J. Am. Chem. Soc. **128:**100–116.
9. **Blount, K. F., F. Zhao, T. Hermann, and Y. Tor.** 2005. Conformational constraint as a means for understanding RNA-aminoglycoside specificity. J. Am. Chem. Soc. **127:**9818–9829.
10. **Botto, R. E., and B. Coxon.** 1983. Nitrogen-15 nuclear magnetic resonance spectroscopy of neomycin B and related aminoglycosides. J. Am. Chem. Soc. **105:**1021–1028.
11. **Carter, A. P., W. M. Clemons, D. E. Brodersen, R. J. Morgan-Warren, B. T. Wimberly, and V. Ramakrishnan.** 2000. Functional insights from the structure of the 30S ribosomal subunit and its interactions with antibiotics. Nature **407:**340–348.
12. **Chambers, H. F.** 2004. Aminoglycosides and spectinomycin, p. 764–772. *In* B. G. Katzung (ed.), Basic and clinical pharmacology, 9th ed. McGraw-Hill, New York, NY.
13. **deHaseth, P. L., T. M. Lohman, and M. T. J. Record.** 1977. Nonspecific interaction of *lac* repressor with DNA: an association reaction driven by counterion release. Biochemistry **16:**4783–4790.
14. **De Stasio, E. A., D. Moazed, H. F. Noller, and A. E. Dahlberg.** 1989. Mutations in 16S ribosomal RNA disrupt antibiotic-RNA interactions. EMBO J. **8:**1213–1216.
15. **Doyle, M. L., G. Louie, P. R. Dal Monte, and T. D. Sokoloski.** 1995. Tight binding affinities determined from thermodynamic linkage to protons by titration calorimetry. Methods Enzymol. **259:**183–194.
16. **Fourmy, D., M. I. Recht, S. C. Blanchard, and J. D. Puglisi.** 1996. Structure of the A site of *Escherichia coli* 16*S* ribosomal RNA complexed with an aminoglycoside antibiotic. Science **274:**1367–1371.
17. **Fourmy, D., S. Yoshizawa, and J. D. Puglisi.** 1998. Paromomycin binding induces a local conformational change in the A-site of 16 S rRNA. J. Mol. Biol. **277:**333–345.
18. **François, B., R. J. Russell, J. B. Murray, F. Aboul-ela, B. Masquida, Q. Vicens, and E. Westhof.** 2005. Crystal structures of complexes between aminoglycosides and decoding A site oligonucleotides: role of the number of rings and positive charges in the specific binding leading to miscoding. Nucleic Acids Res. **33:**5677–5690.
19. **Freire, F., I. Cuesta, F. Corzana, J. Revuelta, C. González, M. Hricovini, A. Bastida, J. Jiménez-Barbero, and J. L. Asensio.** 2007. A simple NMR analysis of the protonation equilibrium that accompanies aminoglycoside recognition: dramatic alterations in the neomycin-B protonation state upon binding to a 23-mer RNA aptamer. Chem. Comm. **2:**174–176.
20. **Fukada, H., and K. Takahashi.** 1998. Enthalpy and heat capacity changes for the proton dissociation of various buffer components in 0.1 M potassium chloride. Proteins Struct. Funct. Genet. **33:**159–166.
21. **Greenberg, W. A., E. S. Priestley, P. S. Sears, P. B. Alper, C. Rosenbohm, M. Hendrix, S.-C. Hung, and C.-H. Wong.** 1999. Design and synthesis of new aminoglycoside antibiotics containing neamine as an optimal core structure: correlation of antibiotic activity with *in vitro* inhibition of translation. J. Am. Chem. Soc. **121:**6527–6541.
22. **Guest, C. R., R. A. Hochstrasser, L. C. Sowers, and D. P. Millar.** 1991. Dynamics of mismatched base pairs in DNA. Biochemistry **30:**3271–3279.
23. **Karimi, R., and M. Ehrenberg.** 1994. Dissociation rate of cognate peptidyl-tRNA from the A-site of hyper-accurate and error-prone ribosomes. Eur. J. Biochem. **226:**355–360.
24. **Kaul, M., C. M. Barbieri, J. E. Kerrigan, and D. S. Pilch.** 2003. Coupling of drug protonation to the specific binding of aminoglycosides to the A site of 16 S rRNA: elucidation of the number of drug amino groups involved and their identities. J. Mol. Biol. **326:**1373–1387.
25. **Kaul, M., C. M. Barbieri, and D. S. Pilch.** 2006. Aminoglycoside-induced reduction in nucleotide mobility at the ribosomal RNA A-site as a potentially key determinant of antibacterial activity. J. Am. Chem. Soc. **128:**1261–1271.
26. **Kaul, M., C. M. Barbieri, and D. S. Pilch.** 2005. Defining the basis for the specificity of aminoglycoside-rRNA recognition: a comparative study of drug binding to the A sites of *Escherichia coli* and human rRNA. J. Mol. Biol. **346:**119–134.
27. **Kaul, M., and D. S. Pilch.** 2002. Thermodynamics of aminoglycoside-rRNA recognition: the binding of neomycin-class aminoglycosides to the A site of 16S rRNA. Biochemistry **41:**7695–7706.
28. **Kozlov, A. G., and T. M. Lohman.** 2000. Large contributions of coupled protonation equilibria to the observed enthalpy and heat capacity changes for ssDNA binding to *Escherichia coli* SSB protein. Proteins Struct. Funct. Genet. **41**(Suppl. 4)**:**8–22.
29. **Manning, G. S.** 1978. The molecular theory of polyelectrolyte solutions with applications to the electrostatic properties of polynucleotides. Q. Rev. Biophys. **11:**179–246.
30. **Miyaguchi, H., H. Narita, K. Sakamoto, and S. Yokoyama.** 1996. An antibiotic-binding motif of an RNA fragment derived from the A-site-related region of *Escherichia coli* 16S rRNA. Nucleic Acids Res. **24:**3700–3706.
31. **Moazed, D., and H. F. Noller.** 1987. Interaction of antibiotics with functional sites in 16S ribosomal RNA. Nature **327:**389–394.
32. **Nordlund, T. M., S. Andersson, L. Nilsson, R. Rigler, A. Gräslund, and L. W. McLaughlin.** 1989. Structure and dynamics of a fluorescent DNA oligomer containing the EcoRI recognition sequence: fluorescence, molecular dynamics, and NMR studies. Biochemistry **28:**9095–9103.
33. **Ogle, J. M., D. E. Brodersen, W. M. Clemons, Jr., M. J. Tarry, A. P. Carter, and V. Ramakrishnan.** 2001. Recognition of cognate transfer RNA by the 30*S* ribosomal subunit. Science **292:**897–902.
34. **Pilch, D. S., M. Kaul, and C. M. Barbieri.** 2005. Ribosomal RNA recognition by aminoglycoside antibiotics. Top. Curr. Chem. **253:**179–204.
35. **Pilch, D. S., M. Kaul, C. M. Barbieri, and J. E. Kerrigan.** 2003. Thermodynamics of aminoglycoside-rRNA recognition. Biopolymers **70:**58–79.
36. **Plum, G. E.** 2000. Optical methods, p. 7.3.1–7.3.17. *In* S. L. Beaucage, D. E. Bergstrom, G. D. Glick, and R. A. Jones (ed.), Current protocols in nucleic acid chemistry, vol. 1. John Wiley & Sons, New York. NY.
37. **Recht, M. I., D. Fourmy, S. C. Blanchard, K. D. Dahlquist, and J. D. Puglisi.** 1996. RNA sequence determinants for aminoglycoside binding to an A-site rRNA model oligonucleotide. J. Mol. Biol. **262:**421–436.
38. **Record, M. T. J., C. F. Anderson, and T. M. Lohman.** 1978. Thermodynamic analysis of ion effects on the binding and conformational equilibria of proteins and nucleic acids: the roles of ion association or release, screening, and ion effects on water activity. Q. Rev. Biophys. **11:**103–178.
39. **Shandrick, S., Q. Zhao, Q. Han, B. K. Ayida, M. Takahashi, G. C. Winters, K. B. Simonsen, D. Vourloumis, and T. Hermann.** 2004. Monitoring the molecular recognition of the ribosomal decoding site. Angew. Chem. Int. Ed. Engl. **43:**3177–3182.
40. **Tsujikawa, L., M. G. Strainic, H. Watrob, M. D. Barkley, and P. L. deHaseth.** 2002. RNA polymerase alters the mobility of an A-residue crucial to polymerase-induced melting of promoter DNA. Biochemistry **41:**15334–15341.
41. **Vicens, Q., and E. Westhof.** 2002. Crystal structure of a complex between the aminoglycoside tobramycin and an oligonucleotide containing the ribosomal decoding A site. Chem. Biol. **9:**747–755.

42. **Vicens, Q., and E. Westhof.** 2003. Crystal structure of geneticin bound to a bacterial 16S ribosomal RNA A site oligonucleotide. J. Mol. Biol. **326:**1175–1188.
43. **Vicens, Q., and E. Westhof.** 2001. Crystal structure of paromomycin docked into the eubacterial ribosomal decoding A site. Structure **9:**647–658.
44. **Wong, C.-H., M. Hendrix, E. S. Priestley, and W. A. Greenberg.** 1998. Specificity of aminoglycoside antibiotics for the A-site of the decoding region of ribosomal RNA. Chem. Biol. **5:**397–406.
45. **Woodcock, J., D. Moazed, M. Cannon, J. Davies, and H. F. Noller.** 1991. Interaction of antibiotics with A- and P-site-specific bases in 16S ribosomal RNA. EMBO J. **10:**3099–3103.
46. **Yoshizawa, S., D. Fourmy, and J. D. Puglisi.** 1999. Recognition of the codon-anticodon helix by ribosomal RNA. Science **285:**1722–1725.
47. **Yoshizawa, S., D. Fourmy, and J. D. Puglisi.** 1998. Structural origins of gentamicin antibiotic action. EMBO J. **17:**6437–6448.
48. **Zhao, F., Q. Zhao, K. F. Blount, Q. Han, Y. Tor, and T. Hermann.** 2005. Molecular recognition of RNA by neomycin and a restricted neomycin derivative. Angew. Chem. Int. Ed. Engl. **44:**5329–5334.